CRYSTAL GROWTH & DESIGN
2008
VOL. 8, NO. 8
2938–2945

Flux-Assisted Thermal Conversion Route to Pore-Free High Crystallinity Magnesium Borate Nanowhiskers at a Relatively Low Temperature

Wancheng Zhu,*[,†,‡] Qiang Zhang,[†] Lan Xiang,*[,†] Fei Wei,[†] Xiaotao Sun,[†] Xianglan Piao,[†] and Shenlin Zhu[†]

Department of Chemical Engineering, Tsinghua University, Beijing 100084, China, and Department of Chemical Engineering, Qufu Normal University, Shandong 273165, China

Received January 14, 2008; Revised Manuscript Received May 8, 2008

ABSTRACT: A flux-assisted thermal conversion route to the pore-free high crystallinity magnesium borate ($Mg_2B_2O_5$) nanowhiskers with a length of 0.47−3.0 μm, diameter of 50−240 nm, and aspect ratio of 5−36 at a relatively low temperature of 650−700 °C (200−350 °C lower than that needed via the traditional method) was developed in this paper. Magnesium borate hydroxide [$MgBO_2(OH)$] nanowhiskers were first prepared by a coprecipitation−hydrothermal approach at 240 °C for 18 h by using $MgCl_2 \cdot 6H_2O$, H_3BO_3 and NaOH (or KOH) as the raw materials and then calcined to produce $Mg_2B_2O_5$ nanowhiskers. The resultant NaCl (or KCl) in the coprecipitation served as the flux and played a key role in the thermal conversion of $MgBO_2(OH)$ nanowhiskers as the transport medium for the rearrangement of structural units of $Mg_2B_2O_5$, leading to the final formation of the pore-free $Mg_2B_2O_5$ nanowhiskers with uniform one-dimensional morphology, high crystallinity, and twin crystal structures.

Introduction

In the last two decades, one-dimensional (1D) nanostructures such as nanotubes, nanowires, nanorods, and nanobelts have been the focus of intensive research for their unique structures, novel properties, and great potential applications.[1–3] A variety of synthetic techniques have been developed for the preparation of 1D nanostructures, among which chemical vapor deposition (CVD) has been widely used for the synthesis of metal oxide nanobelts[2] and nanowires,[3] particularly for its versatility[3,4] and high crystallinity.[5] However, CVD also faces the problems such as high energy consumption, difficulty in scaling-up,[4] and broad distributions of the size and morphology of the product. Molten salt synthesis (MSS) is another widely used technique for preparing ceramic powders with whiskerlike, needlelike, and platelike morphologies; nevertheless, MSS generally leads to diameters ranging from several to tens of micrometers, and it is difficult to obtain nanoparticles or nanowhiskers.[6,7]

In contrast, hydrothermal technology has emerged as a thriving method for the synthesis of 1D nanostructures in the past decade[8–11] because of its advantages over other conventional processes, such as its energy savings, better control of nucleation and shape, and lower temperature of operation, etc.[12] However, hydrothermal synthesis readily results in 1D hydroxyl or hydrated compounds, and subsequent calcination or annealing is usually needed to obtain the corresponding 1D anhydrous compound, for example, oxides. One-dimensional nanostructured transition and rare earth metal oxides such as Co_3O_4 nanorods,[7] Eu_2O_3 nanorods,[13] Tb_4O_7 and Y_2O_3 nanotubes,[14,15] Y_2O_3:Eu nanobelts,[16] Dy_2O_3 nanotubes,[17] and $MnO_2/Mn_2O_3/Mn_3O_4$ nanorods[18] with well-preserved 1D morphology and high crystallinity have been synthesized via the calcination of the corresponding 1D precursors, probably due to the relatively low decomposition temperature and characteristics of the transition and rare earth metal compounds. Nevertheless, in more cases such as MgO nanorods[19] and Al_2O_3 nanorods,[20,21] etc., pores, severe deformation, and even rupture readily occurred in the thermal conversion process due to the dehydration or devolatilization.[15,19–26] Many efforts have been made to improve the 1D morphology and crystallinity of the calcined products; for example, sintering at low temperature[14,16,18,24,25] and adaptation of the multistep heating procedure[19] could weaken the deformation and thus reduce the rupture, and the addition of the NaCl flux and nonyl pheyl ether[9] could promote 1D growth of the nanostructures with good dispersion.[7,26–28] It is, however, still a challenge to avoid deformation and degradation of the crystallinity of the calcined product due to the pores generated from the elimination of the volatile components.[19–21,23–26]

One-dimensional nanostructured magnesium borates, including MgB_4O_7 nanowires,[29] $Mg_3B_2O_6$ nanotubes[30] and nanobelts,[31] $Mg_2B_2O_5$ nanowires,[32,33] nanorods,[34] and whiskers,[35–37] etc., have been paid much attention in recent years for their potential usage as reinforcements in the electronic ceramics,[29] wide band gap semiconductors,[32] antiwear additive,[33] and plastics or aluminum/magnesium matrix alloys.[37] Traditionally, 1D mirco-/nanostructured magnesium borates have been prepared via CVD[29–34] or MSS routes[35–37] at high temperature within 850−1250 °C or using a solution-based method under supercritical conditions (500−600 °C, 200−1000 bar, and 14 days).[38] Although 1D $Mg_2B_2O_5$ nanostructures synthesized by the above methods exhibited high crystallinity, problems such as high energy consumption, coexistence of the particulate agglomerates,[29,31,35–37] and relatively rigorous experimental conditions[30,32,38] still needed to be solved.

$MgBO_2(OH)$ could be converted to irregular particulate $Mg_2B_2O_5$ at a temperature above 610 °C,[38] revealing the possibility of synthesizing 1D $Mg_2B_2O_5$ nanostructures from the thermal conversion of 1D $MgBO_2(OH)$ nanostructures. Recently, 1D $MgBO_2(OH)$ nanostructures have been synthesized under hydrothermal conditions;[39–41] however, little work has focused on the thermal conversion of 1D $MgBO_2(OH)$ to 1D $Mg_2B_2O_5$ to date. In our previous work, uniform $MgBO_2(OH)$ nanowhiskers have been synthesized via a coprecipitation−hydrothermal reaction route;[41] here, we report, for the first time

* To whom correspondence should be addressed. Tel: +86-10-62788984. Fax: +86-10-62772051. E-mail: zhuwc04@mails.tsinghua.edu.cn (W.Z.) and xianglan@mail.tsinghua.edu.cn (L.X.).
† Tsinghua University.
‡ Qufu Normal University.

10.1021/cg800050u CCC: $40.75
Published on Web 07/10/2008

to the best of our knowledge, a flux-assisted thermal conversion route to the pore-free high crystallinity $Mg_2B_2O_5$ nanowhiskers at a relatively low temperature of 650−700 °C based on the former solution synthesis. The resultant NaCl (or KCl) in the coprecipitation served as the flux and played a key role in the thermal conversion of $MgBO_2(OH)$ nanowhiskers to the pore-free $Mg_2B_2O_5$ nanowhiskers with uniform 1D morphology, high crystallinity, and twin crystal structures. The flux-assisted solution-based thermal conversion route was also helpful for the preparation of other pore-free high crystallinity 1D nanostructures from the corresponding 1D nanostructured precursors.

Experimental Section

$MgBO_2(OH)$ nanowhiskers were synthesized by the coprecipitation of NaOH (or KOH), $MgCl_2$, and H_3BO_3 solutions at room temperature with the molar ratio of Mg:B:Na (or K) as 2:3:4, followed by the hydrothermal treatment of the slurry ($Mg_7B_4O_{13}\cdot 7H_2O$) at 240 °C for 18.0 h.[41] The dried hydrothermal product derived from the filtration of the hydrothermal slurry, with or without additional washing, was then transferred into a porcelain boat located in a horizontal quartz tube furnace, heated (1.0 °C min^{-1}) to 650−700 °C, and kept in an isothermal state for 2.0 h. After the thermal conversion, the samples were cooled down to room temperature naturally within the tube furnace (denoted as N cooling hereafter), then collected, washed with distilled water, and finally dried at 105 °C for 12.0 h. To investigate the effect of flux on the formation of $Mg_2B_2O_5$ nanowhiskers, unwashed $MgBO_2(OH)$ was calcined at a designed temperature, then taken out of the tube furnace directly with a rapid cooling to room temperature (denoted as R cooling hereafter), and finally collected without washing for further characterization.

The structure of the sample was identified by the X-ray powder diffractometer (XRD, D8-Advance, Bruker, Germany) using Cu Kα radiation (λ = 1.54178 Å), a fixed power source (40.0 kV, 40.0 mA), and an aligned silicon detector. The morphology, microstructure, and composition of the samples were examined by field emission scanning electron microscopy (FESEM, JSM 7401F, JEOL, Japan) operated at an accelerating voltage of 1.0 kV attached with an X-ray energy dispersive spectrometer (EDS, EDAX Genesis 2000, EDAX, United States) and high-resolution transmission electron microscopy (HRTEM, JEM-2010, JEOL, Japan) performed at an accelerating voltage of 120.0 kV equipped with an EDS (INCA Energy TEM, Oxford Instruments, United Kingdom) and a charge-coupled device (CCD) camera (Orius SC 1000, Gatan, United States). The relative contents of Na and Cl in the samples were analyzed by the inductively coupled plasma optical emission spectrometer (ICP-OES, IRIS Intrepid II XSP, Thermo Elemental, United States) and ion chromatography (IC, ICS-3000, DIONEX, United States), respectively. The size distribution of the nanowhiskers was estimated by directly measuring about 200 particles from the typical FESEM images. The N_2 adsorption−desorption isotherms were measured at 77 K using a chemisorption−physisorption analyzer (Autosorb-1-C, Quantachrome, United States) after the samples had been outgassed at 300 °C for 60 min. The specific surface area was calculated from the adsorption branches in the relative pressure range of 0.05−0.25 using a multipoint Brunauer−Emmett−Teller (BET) method, and the pore size distribution was evaluated from the nitrogen adsorption isotherm using the Barrett−Joyner−Halenda (BJH) method.

Results and Discussion

Monoclinic $MgBO_2(OH)$ (PDF No. 39-1370) nanowhiskers[41] were synthesized by the coprecipitation at room temperature (eq 1) and subsequent hydrothermal synthesis (eq 2) as follows:

$$7MgCl_2 + 4H_3BO_3 + 14NaOH \rightarrow Mg_7B_4O_{13}\cdot 7H_2O(s) + 14NaCl + 6H_2O \quad (1)$$

$$Mg_7B_4O_{13}\cdot 7H_2O(s) + 3H_3BO_3 \rightarrow 7MgBO_2(OH)(s) + 8H_2O \quad (2)$$

Figure 1 shows the FESEM images of the washed and unwashed hydrothermal products. Dispersive uniform $MgBO_2$-

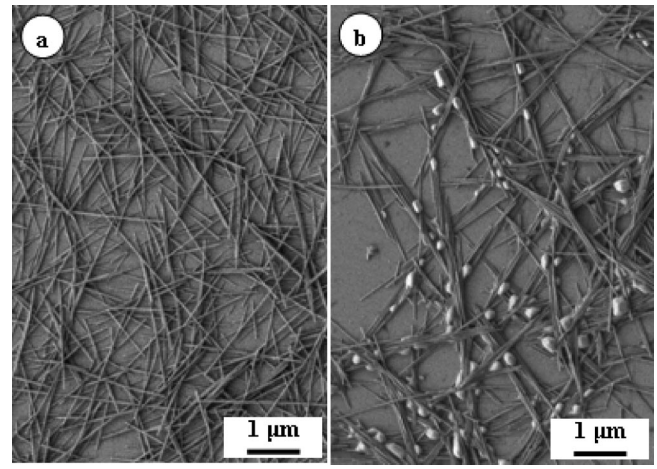

Figure 1. FESEM images of the washed (a) and unwashed (b) $MgBO_2(OH)$ nanowhiskers.

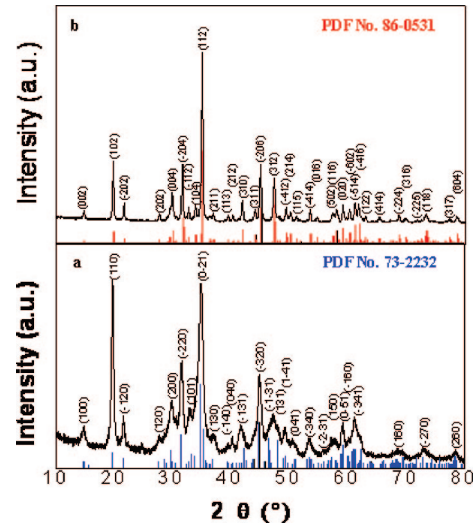

Figure 2. XRD patterns of the $Mg_2B_2O_5$ nanowhiskers calcined with or without NaCl. (a) Triclinic phase calcined in the absence of NaCl (vertical line, standard pattern of the triclinic $Mg_2B_2O_5$). (b) Monoclinic phase calcined in the presence of NaCl (vertical line, standard pattern of the monoclinic $Mg_2B_2O_5$).

(OH) (Figure S1a in the Supporting Information) nanowhiskers with a diameter of 20−50 nm and a length of 0.5−3 μm (Figure 1a) were obtained after washing (i.e., in the absence of NaCl), whereas bundles of $MgBO_2(OH)$ nanowhiskers that coexisted with irregular block particles (Figure 1b) were acquired without washing (i.e., in the presence of NaCl). The XRD pattern of the unwashed hydrothermal product (Figure S1b in the Supporting Information) and the EDS spectrum recorded from those particles during the SEM observation definitely indicated the irregular block particles as NaCl (Figure S2 in the Supporting Information), taking into consideration the background element Si from the employed Si substrate and Mg and O originating from the ambient 1D $MgBO_2(OH)$ nanowhiskers.

The XRD patterns of the calcined products are shown in Figure 2. $Mg_2B_2O_5$ was obtained via the thermal conversion of $MgBO_2(OH)$ due to the dehydration (eq 3):

$$2MgBO_2(OH)(s) \rightarrow Mg_2B_2O_5(s) + H_2O(g) \quad (3)$$

Dehydration of the washed $MgBO_2(OH)$ nanowhiskers resulted in $Mg_2B_2O_5$ with a major triclinic phase [PDF No. 73-

2232, space group: $P\bar{1}(2)$] with weak crystallinity (Figure 2a), whereas dehydration of the unwashed $MgBO_2(OH)$ nanowhiskers led to a pure monoclinic phase $Mg_2B_2O_5$ [PDF No. 86-0531, space group: $P21/c(14A)$] with high crystallinity (Figure 2b). The cell parameters correlated from the step-scanned XRD data of the product calcined in the presence of NaCl were as follows: $a = 9.202$ Å, $b = 3.124$ Å, $c = 12.318$ Å, and $\beta = 104.344°$, which were consistent with the standard value of the monoclinic $Mg_2B_2O_5$ ($a = 9.197$ Å, $b = 3.1228$ Å, $c = 12.303$ Å, and $\beta = 104.26°$). Monoclinic $Mg_2B_2O_5$[34,36] and triclinic $Mg_2B_2O_5$[32,33,44] were also obtained by former researchers, whereas in our case the presence of NaCl during the calcination promoted the formation of the monoclinic phase $Mg_2B_2O_5$ with improved crystallinity. Although the role of the NaCl in promotion of the monoclinic phase $Mg_2B_2O_5$ was still unclear, the present study presented a facile NaCl-assisted thermal conversion approach for 1D nanostructures of the monoclinic $Mg_2B_2O_5$ with high crystallinity.

Figure 3 shows the typical morphology and size distribution of the $Mg_2B_2O_5$ nanowhiskers calcined with or without NaCl. $Mg_2B_2O_5$ nanowhiskers (length, 0.2−2.0 μm; diameter, 15.0−45.0 nm) with a relatively coarse surface and a few unavoidable mesopores (Figure 3a,b) were obtained after calcination in the absence of NaCl, verifying the relatively weak crystallinity (Figure 2a). $Mg_2B_2O_5$ nanowhiskers calcined in the presence of NaCl (Figure 3c) with a length of 0.47−3.0 μm (average, 1.57 μm), a diameter of 50−240 nm (average, 99 nm), and an aspect ratio of 5−36 (average, 16) exhibited uniform ultrafine columnlike morphology with explicitly cut edges and a typical rectangular cross-section (Figure 3d), reconfirming the high crystallinity (Fiugre 2b). In contrast with other 1D micro/nanostructures of $Mg_2B_2O_5$, the present nanowhiskers were shorter than the whiskers[35–37] and nanowires,[32,33] whereas they were longer than the nanorods,[34] thicker than the nanowires, but much thinner than the whiskers. Moreover, $Mg_2B_2O_5$ nanowhiskers reported here exhibited a narrow distribution of both the length and the aspect ratio (Figure 3e,f). Differing from the agglomerates generally occurred in the $Mg_2B_2O_5$ whiskers prepared by the MSS method due to the mass use of the flux;[35–37] uniform $Mg_2B_2O_5$ nanowhiskers in either monodispersive manner or side-by-side adhered manners were synthesized by the present NaCl-assisted thermal conversion route, which would greatly facilitate the further surface modification and potential applications. Besides, as compared with the $Mg_2B_2O_5$ whiskers[35–37] prepared by the MSS method (850−900 °C) or the $Mg_2B_2O_5$ nanowires[32,33] synthesized by the CVD method (850−1250 °C), the present $Mg_2B_2O_5$ nanowhiskers were obtained at a relatively lower temperature of 650−700 °C, promising much lower energy consumption.

Figure 4 shows the typical TEM image, EDS spectrum, SAED pattern, and HRTEM image of the $Mg_2B_2O_5$ nanowhiskers calcined in the presence of NaCl. $Mg_2B_2O_5$ nanowhiskers with a straight smooth surface were formed, and no pores were detected after the elimination of the volatile water molecules via calcination (Figure 4a), indicating the high crystallinity and well-preserved 1D morphology obtained in the presence of NaCl, in contrast with the $Mg_2B_2O_5$ nanowhiskers with a few unavoidable mesopores (Figure 3b) and also the general deformation and sometimes even severe rupture of the calcined 1D nanostructures via the solution-based thermal conversion route in the absence of flux.[19,23]

The EDS spectrum (Figure 4b) obtained from the circled area containing dense nanowhiskers in Figure 4a indicated that the nanowhiskers were composed of Mg, B, and O (the occurrences

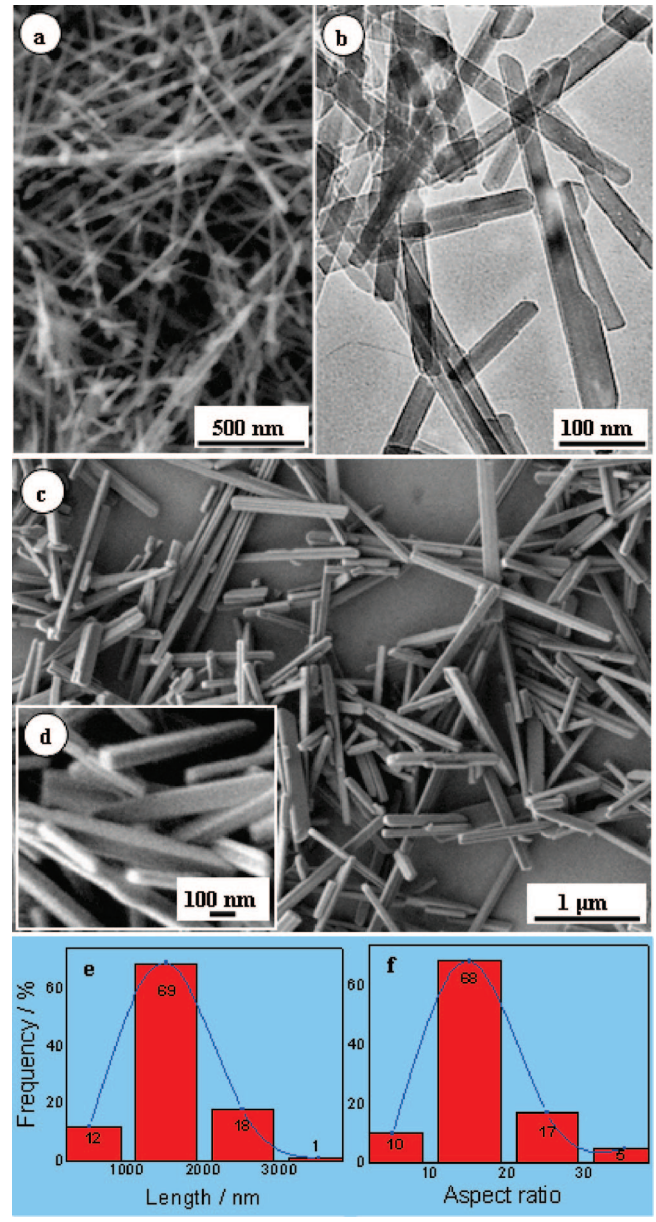

Figure 3. FESEM images (a, c, and d), TEM image (b), and size distribution (e and f) of the $Mg_2B_2O_5$ nanowhiskers calcined in the absence (a and b) and presence (c−f) of NaCl.

of C and Cu were attributed to the carbon-coated TEM copper grid). The SAED pattern (Figure 4c) recorded from the $[24\bar{1}]$ zone axis, corresponding to an individual nanowhisker labeled by the rectangular area (Figure 4a), revealed that the nanowhisker had a longitudinal direction parallel to the (102) planes. In addition, another set of diffraction spots with relatively dim brightness coexisted in the SAED pattern, which implied a possible existence of the twin crystal structures. Corresponding to the rectangular region in the individual nanowhisker in Figure 4a, three interplanar spacings in various directions (0.249, 0.396, and 0.254 nm) were detected from the legible lattice fringes (Figure 4d), quite similar to those of the $(\bar{2}12)$, $(\bar{2}02)$, and (112) planes of the monoclinic $Mg_2B_2O_5$, respectively, revealing the high crystallinity and axial direction of the $Mg_2B_2O_5$ nanowhiskers parallel to the $(\bar{2}02)$ planes. The $Mg_2B_2O_5$ nanowhisker had an axial direction simultaneously parallel to the (102) planes and $(\bar{2}02)$ planes, which exclusively indicated the axial direction of the $Mg_2B_2O_5$ nanowhiskers along the *b*-axis, that is, the [010] direction, in agreement with the preferential growth of the

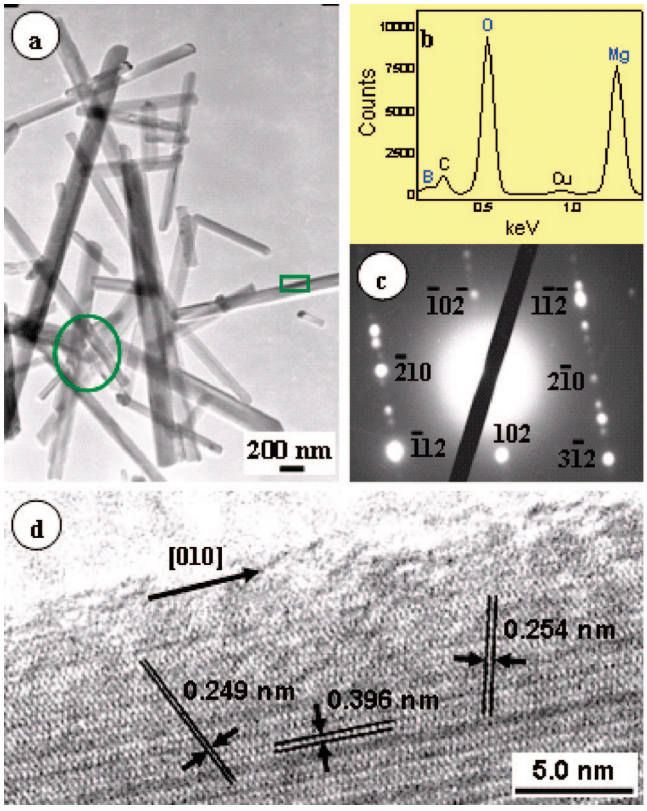

Figure 4. TEM image (a), EDS spectrum (b), SAED pattern (c), and HRTEM image (d) of the pore-free high crystallinity $Mg_2B_2O_5$ nanowhiskers calcined in the presence of NaCl.

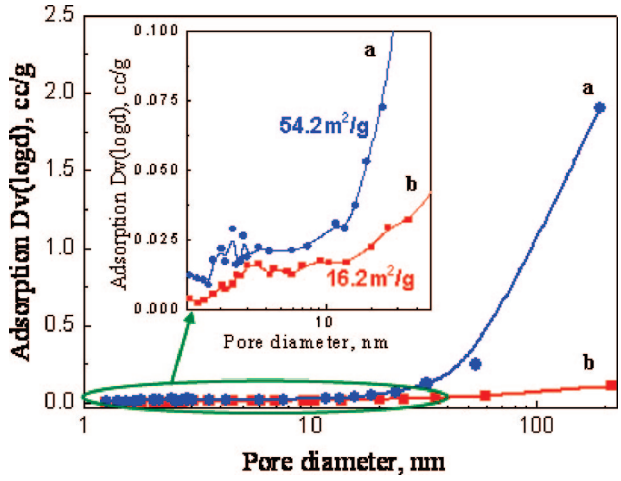

Figure 5. Pore size distribution and specific surface area of the $Mg_2B_2O_5$ nanowhiskers calcined in the absence (a) and presence (b) of NaCl, with a specific surface area of 54.2 and 16.2 m^2/g, respectively.

natural suanite ($Mg_2B_2O_5$) along the *b*-axis.[42] Furthermore, the acquisition of the HRTEM image and SAED pattern from almost the same selected area revealed not only the high crystallinity but also the excellent thermal stability of the $Mg_2B_2O_5$ nanowhiskers under electron beam irradiation.

The pore size distribution and specific surface area were measured to further investigate the possible existence of pores in the bulk of the $Mg_2B_2O_5$ nanowhiskers calcined in the absence and presence of NaCl, as shown in Figure 5. For the $Mg_2B_2O_5$ nanowhiskers calcined in the absence of NaCl (Figure 5a), a slight adsorbance of N_2 was detected within the pore diameter range of 15 nm owing to a few mesopores in the bulk of

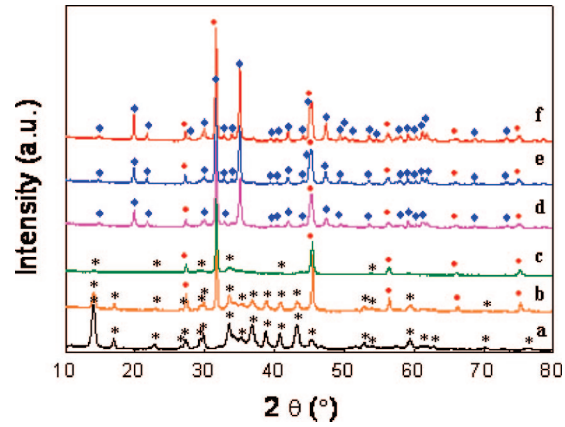

Figure 6. XRD patterns of the washed (a) and unwashed (b−f) products. (a) Hydrothermal, (b) hydrothermal, (c) calcined at 550 °C/R cooling, (d) calcined at 650 °C/R cooling, (e) calcined at 700 °C/R cooling, and (f) calcined at 700 °C/N cooling; $MgBO_2(OH)$ (*), $Mg_2B_2O_5$ (◆), and NaCl (●).

nanowhiskers originating from the dehydration, and the adsorbance went up dramatically when the pore diameter exceeded 15 nm due to the stack of the nanowhiskers. However, for the $Mg_2B_2O_5$ nanowhiskers calcined in the presence of NaCl (Figure 5b), much less adsorbance of N_2 was observed and just increased a little within the pore diameter range of 200 nm for a few pores that existed in the bulk of the nanowhiskers. Correspondingly, the specific surface area of the nanowhiskers decreased from 54.2 m^2/g (in the absence of NaCl) to 16.2 m^2/g (in the presence of NaCl), as a result of the disappearance of the pores and the increase in the diameter of the nanowhiskers.

Pore-free $Mg_2B_2O_5$ nanowhiskers with uniform 1D morphology and high crystallinity have been synthesized by the NaCl-assisted thermal conversion route at a relatively low temperature; nevertheless, how NaCl could play such a key role in promoting the crystallinity and eliminating the pores still needed to be probed. Figure 6 shows the variation of the chemical composition and crystallinity of the hydrothermal as well as the calcined products obtained in the presence of NaCl. As compared with the washed $MgBO_2(OH)$ nanowhiskers (Figure 6a), the unwashed hydrothermal product (Figure 6b) exhibited strong diffraction of NaCl, resulting in the diffraction peaks of $MgBO_2(OH)$ submerged in a sense. $MgBO_2(OH)$ with poor crystallinity for gradual dehydration coexisted with NaCl in the unwashed powder, which was calcined at 550 °C and then followed by R cooling (Figure 6c). The crystallinity degradation of the $MgBO_2(OH)$ nanowhiskers calcined in the presence of NaCl was quite similar to that in the absence of NaCl when the temperature was below 550 °C. The monoclinic $Mg_2B_2O_5$ was found at 650 °C in the presence of NaCl (Figure 6d), different from the triclinic $Mg_2B_2O_5$ emerged in the thermal conversion of the washed $MgBO_2(OH)$ nanowhiskers at the same temperature. The crystallinity of the monoclinic $Mg_2B_2O_5$ got higher when the temperature increased to 700 °C (Figure 6e) and further improved by the N cooling of the final product (Figure 6f). Hence, the presence of NaCl neither changed the conversion temperature from $MgBO_2(OH)$ to $Mg_2B_2O_5$ nor led to other intermediate phase containing boron during the calcination process.

The crystallite size of the $Mg_2B_2O_5$ nanowhiskers (Figure 6d−f) was evaluated via the Scherrer equation.[45] With the variation of the temperature/cooling procedure from 650 °C/R cooling to 700 °C/R cooling and to 700 °C/N cooling, the crystallite size in the direction perpendicular to the (102) planes

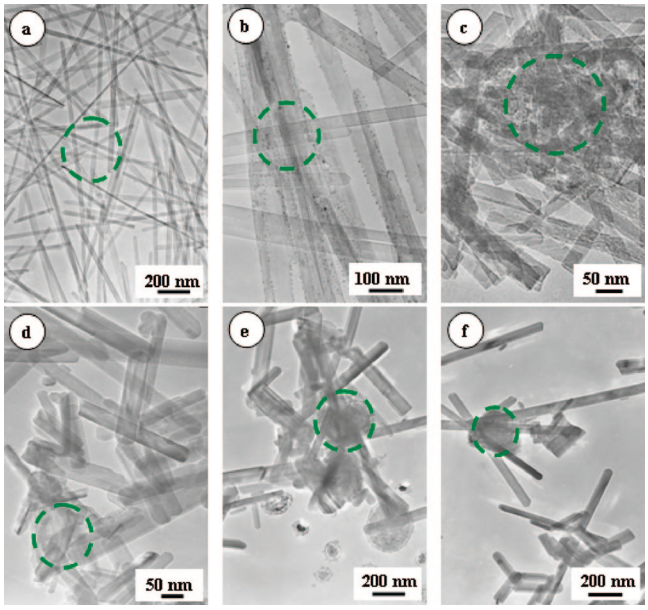

Figure 7. TEM images of the washed (a) and unwashed (b−f) products. (a) Hydrothermal, (b) hydrothermal, (c) calcined at 550 °C/R cooling, (d) calcined at 650 °C/R cooling, (e) calcined at 700 °C/R cooling, and (f) calcined at 700 °C/N cooling.

(located at approximately $2\theta \approx 20°$ in the XRD pattern) L_{102} changed from 31.6 to 34.3 nm and finally to 44.5 nm, respectively, indicating the gradual growth of the $Mg_2B_2O_5$ nanowhiskers in the diameter direction. The crystallite size of the final obtained $Mg_2B_2O_5$ nanowhiskers (44.5 nm) was quite similar to the diameter of the hydrothermal synthesized $MgBO_2(OH)$ nanowhiskers[41] but approximately one-half of the average diameter of the $Mg_2B_2O_5$ nanowhiskers (Figure 3c), which implied the possible side-by-side coalescence growth of the $Mg_2B_2O_5$ nanowhiskers via the present NaCl-assisted thermal conversion route.

Figure 7 further shows the morphology and congregating behavior of the NaCl in the unwashed nanowhiskers corresponding to those presented in Figure 6. In contrast with the washed uniform dispersive $MgBO_2(OH)$ nanowhiskers (Figure 7a), most and especially those bundled $MgBO_2(OH)$ nanowhiskers were attached by the nanoparticles (Figure 7b), which were proved as NaCl by the analysis of the EDS spectra (Figure 8a,b) recorded from the corresponding circled areas of the washed and unwashed nanowhiskers (Figure 7a,b). Taking into consideration the background C and Cu in the carbon-coated copper grid, the calcined nanowhiskers under different conditions in the presence of NaCl (Figure 7c−f) were all composed of Mg, B, O, Na, and Cl (Figure 8c−f). Many pores existed in the bulk of the $MgBO_2(OH)$ nanowhiskers calcined at 550 °C (Figure 7c), whereas they completely disappeared at temperatures above 650 °C (Figure 7d−f). Meanwhile, NaCl tended to be congregated with each other either on the surfaces of the $Mg_2B_2O_5$ nanowhiskers or in a dissociative state after the pores disappeared (Figure 7d−f). A pure phase of the pore-free dispersive $Mg_2B_2O_5$ nanowhiskers could be obtained by facile and thorough cleaning with deionized water and also proved the final existence state of the NaCl after calcination. NaCl has been found as an effective flux agent in the thermal conversion route to some oxide nanorods at the temperature above its melting point (800 °C).[7,26−28] The present work showed that NaCl had begun to take effect at a temperature lower than its melting point; thus, it was deduced that NaCl nanoparticles attached on the surfaces of $MgBO_2(OH)$ nanowhiskers might melt at 550−650 °C due to the small size effect and then serve as a flux for the improvement of the crystallinity and elimination of the pores, similar to the effect of NaCl as a liquid medium favorable for the homogeneous distribution and growth of the whiskers or nanorods.[7,26,28]

To better understand the role of the NaCl in the formation of the pore-free $Mg_2B_2O_5$ nanowhiskers, the unwashed $MgBO_2(OH)$ nanowhiskers were further investigated by an in situ TEM observation. Block crystalline NaCl in the selected area gradually melted into NaCl nanoparticles under bombardment of the electron beam (Figure 9a), then collapsed into smaller nanoparticles and dispersed onto the surfaces of the nanowhiskers (Figure 9b), and finally formed a fluctuated viscous molten film expanded onto the surfaces, leading to the side aggregation and further fusion of the adjacent nanowhiskers in some cases (e.g., elliptical region in Figure 9c) during the calcination. With the intensity of the electron beam enhanced and the irradiation time prolonged, pores gradually emerged and grew in the section without coverage of the molten NaCl of the $MgBO_2(OH)$ nanowhiskers because of the gradual dehydration, whereas no pores were observed in the section covered with the molten NaCl of the nanowhiskers; the covered section significantly shrank due to the promoted recrystallization, resulting in a thinner diameter. This phenomenon was confirmed by the successively captured images from the video recorded by the CCD camera during the in situ TEM observation (Figure S3 in the Supporting Information). It was also observed that the molten NaCl gently disappeared after a long time irradiation, indicating the evaporation of the NaCl under long-time electron beam irradiation. Similar behavior of the NaCl has also emerged in the calcination process. The inner surface of the quartz tube turned white after calcination, and the content of the Na and Cl in the unwashed powders generally decreased with the increase in the calcination temperature (Table 1), confirming the evaporation of the NaCl in the course of the calcination. Moreover, the observed stable 1D morphology of the nanowhiskers throughout the melting process of the block NaCl at a temperature above 800 °C (Figure 9a−c) indicated the preservation of the 1D morphology of the nanowhiskers via the present NaCl-assisted thermal conversion route at a temperature below 700 °C (Figure 7b−f).

Although the side aggregation and fusion of the adjacent nanowhiskers in the presence of NaCl did not demonstrate a remarkable effect on the final porosity of the calcined $Mg_2B_2O_5$ nanowhiskers, it might contribute to the side-by-side coalescence growth of the $Mg_2B_2O_5$ nanowhiskers. The TEM image, SAED pattern, and HRTEM image recorded from the same individual nanowhisker (Figure 10a−c) showed that the nanowhisker contained a twin plane in the middle, parallel to the longitudinal axis of the nanowhisker (i.e., [010] direction), and the two interplanar spacings (0.890 and 0.893 nm) further indicated the mirror being positioned parallel to (100) planes, similar to the twin crystal structures that existed in the nanowires of Ag[46] and CuO.[47] The twin crystal structures could well interpret the side-by-side adherence of the $Mg_2B_2O_5$ nanowhiskers in the SEM observation (Figure 3c), as well as the statistically obtained diameter of the calcined $Mg_2B_2O_5$ nanowhiskers approximately twice of that evaluated by the Scherrer equation. With the progress of the NaCl-assisted recrystallization, the pores generated from previous dehydration were healed and the crystallinity of the final calcined $Mg_2B_2O_5$ nanowhiskers could thus be greatly improved.

An extended experiment showed that, with additional NaCl added into the system, more side-by-side coalescence of the nanowhiskers as well as distinct agglomerates were obtained.

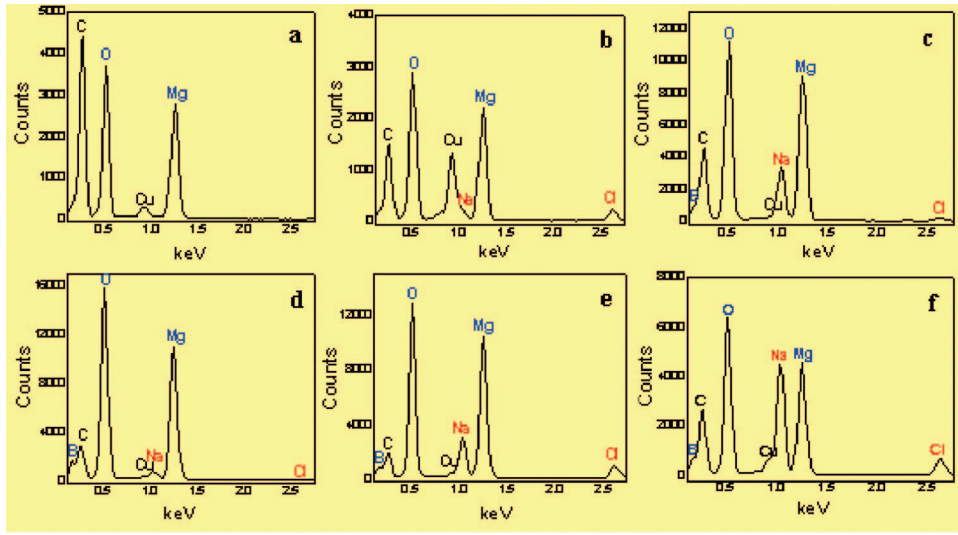

Figure 8. EDS spectra of the washed (a) and unwashed (b−f) products. (a) Hydrothermal, (b) hydrothermal, (c) calcined at 550 °C/R cooling, (d) calcined at 650 °C/R cooling, (e) calcined at 700 °C/R cooling, and (f) calcined at 700 °C/N cooling.

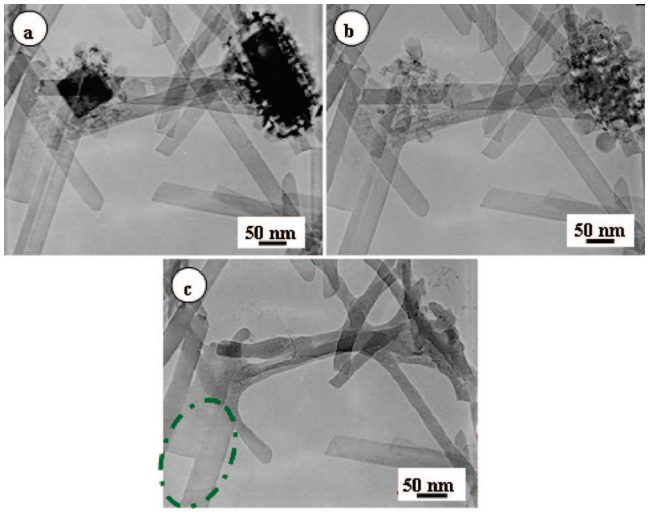

Figure 9. Melting behavior of the NaCl in the unwashed $MgBO_2(OH)$ nanowhiskers under the bombardment of the electron beam. Block NaCl gradually melted into nanoparticles (a), further collapsed into smaller nanoparticles and dispersed on the surfaces (b), and finally formed a fluctuated film expanded onto the surfaces leading to the side-by-side coalescence of the adjacent nanowhiskers as indicated by the elliptical area (c).

Table 1. Variation of the Content of the Na and Cl in the Unwashed Calcined Powders

samples	descriptions	content of Na (wt %)	content of Cl (wt %)
1	hydrothermal	15.83	19.20
2	calcined at 550 °C/R cooling	13.44	19.48
3	calcined at 700 °C/R cooling	11.15	15.69
4	calcined at 700 °C/N cooling	9.74	13.39

Besides NaCl, KCl was also found to be effective for the preparation of monoclinic $Mg_2B_2O_5$ nanowhiskers with high crystallinity and no pores when KOH was employed instead of NaOH as the raw material, with other conditions kept the same. It was believed that KCl had played the same role with NaCl as a flux in promoting the formation of the pore-free $Mg_2B_2O_5$ nanowhiskers during calcination.

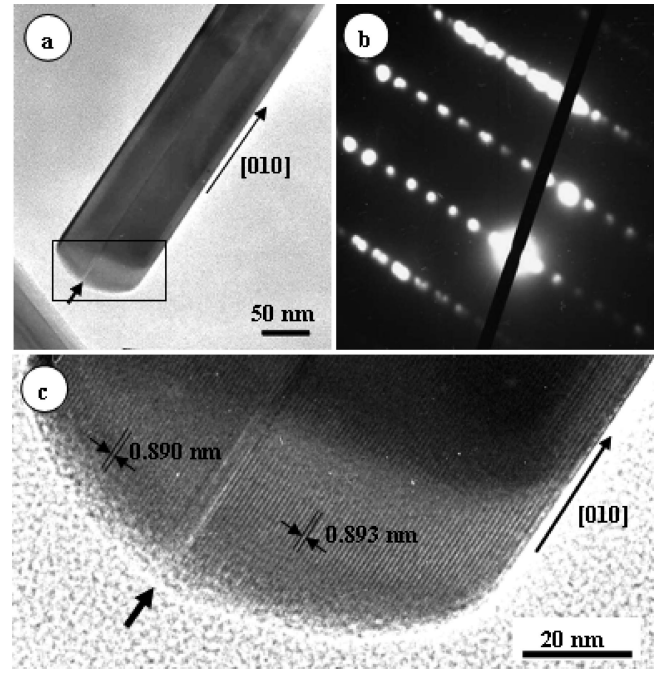

Figure 10. TEM image (a), SAED pattern (b), and HRTEM image corresponding to the rectangular framed end (c) of the $Mg_2B_2O_5$ nanowhisker, with a twin plane parallel to the longitudinal axis and the mirror being positioned parallel to (100) planes (indicated by an arrow).

On the basis of the former results, the formation mechanism of the pore-free high crystallinity $Mg_2B_2O_5$ nanowhiskers with uniform 1D morphology via the flux-assisted thermal conversion route could thus be deduced and illustrated, as shown in Figure 11. After hydrothermal synthesis, flux nanoparticles (NaCl or KCl) tended to be attached onto the surfaces of the $MgBO_2(OH)$ nanowhiskers (Figures 7b and 11a). With the temperature increased to 550 °C, the combination of the OH and O atoms and further elimination of the H_2O molecules from the unit cell of $MgBO_2(OH)$ resulted in a magnitude of mesopores in the $MgBO_2(OH)$ nanowhiskers, which could coalesce into bigger ones and even microchannels owing to the successive heating, dehydration, and coalescence (Figures 7c and 11b). When the

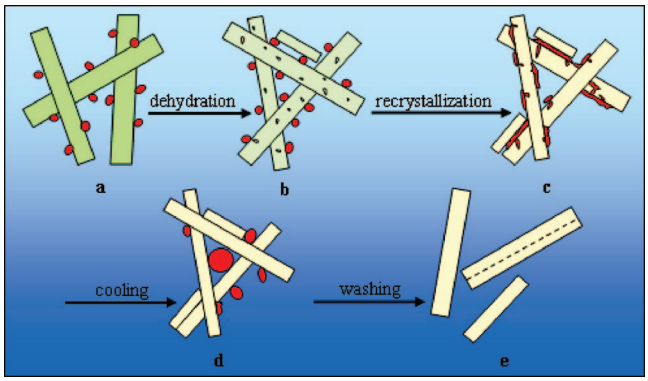

Figure 11. Formation mechanism of the pore-free high crystallinity $Mg_2B_2O_5$ nanowhiskers via the flux-assisted thermal conversion route. (a) Crystalline $MgBO_2(OH)$ nanowhiskers with attached flux nanoparticles. (b) Mesoporous $Mg_2B_2O_5$ nanowhiskers with attached flux nanoparticles after dehydration. (c) $Mg_2B_2O_5$ nanowhiskers with melting flux infiltrating into the vacancies through microchannels during recrystallization. (d) Pore-free $Mg_2B_2O_5$ nanowhiskers with congregated flux particles. (e) Dispersive pore-free high crystallinity $Mg_2B_2O_5$ nanowhiskers after washing (dashed, a twin plane).

system was heated to a certain temperature within the range of 550−650 °C, the attached flux nanoparticles gradually melted and expanded into a fluctuated film, and the molten flux could readily flow into the vacancies on the surfaces of mesoporous $Mg_2B_2O_5$ nanowhiskers and then penetrate into the depth of the nanowhiskers via the microchannels. The molten flux reached the inner pores, and microchannels could thus serve as a transport medium for the rearrangement of the structural units Mg^{2+} and $[B_2O_5]^{4-}$, that is, recrystallization, when the system was heated to 650−700 °C. With the assistance of the flux transport medium, which in other words is like a swimming pool, the building units of Mg^{2+} and $[B_2O_5]^{4-}$ could be readily transported, or swim to the appropriate position, and the new lattice of monoclinic $Mg_2B_2O_5$ could therefore be easily built (Figure 11c). Pores and vacancies were gradually healed with the progress of recrystallization, and the molten flux was migrated to the ambient vacancies and finally extruded out from the bulk of the $Mg_2B_2O_5$ nanowhiskers. The expelled molten flux could then recrystallize in the course of cooling after calcination, then congregate with each other or enrich on the surfaces of the calcined nanowhiskers (Figure 11d). Finally, the pure phase of pore-free dispersive $Mg_2B_2O_5$ nanowhiskers was obtained via a facile thorough cleaning with deionized water (Figure 11e), which reconfirmed not only the role of flux as a transport medium within the pores and microchannels during the recrystallization process without dropping the crystal lattice of $Mg_2B_2O_5$ (Figure 2b) but also the restoration of flux back to the surfaces of the calcined nanowhiskers after cooling. As a matter of fact, the general decrease in the content of the Na and Cl in the unwashed powders with the increase in the calcination temperature (Table 1) also verified the migration of the flux from the inner to the exterior of the calcined nanowhiskers after cooling. The molten flux on the one hand played the key role in the rearrangement of the mesoporous $Mg_2B_2O_5$ at recrystallization stage (650−700 °C)[43] and resulted in the pore-free high crystallinity $Mg_2B_2O_5$ nanowhiskers with uniform 1D morphology and on the other hand brought about the side-by-side coalescence growth and twin crystal structures in some cases. Although NaCl and KCl could both promote the formation of the pore-free $Mg_2B_2O_5$ nanowhiskers, NaCl was likely preferred for its lower cost and easier separation.

Conclusion

In summary, a flux-assisted solution-based thermal conversion route was developed to form the pore-free high crystallinity $Mg_2B_2O_5$ nanowhiskers (length, 0.47−3.0 μm; diameter, 50−240 nm; and aspect ratio, 5−36), in which $MgBO_2(OH)$ nanowhiskers were synthesized under hydrothermal conditions (240 °C, 18 h) and followed by the calcination at a relatively low temperature of 650−700 °C (200−350 °C lower than that of the literature) under a slow heating rate (1.0 °C min^{-1}), with the resultant NaCl (or KCl) nanoparticles as the flux. The existence of the flux on the one hand played a key role in the thermal conversion of the $MgBO_2(OH)$ nanowhiskers as the transport medium for the rearrangement of the structural units of $Mg_2B_2O_5$, leading to the final formation of the pore-free $Mg_2B_2O_5$ nanowhiskers with high crystallinity and on the other hand resulted in the twin crystal structures, the formation process and mechanism of which still need to be further investigated. Considering the general formation of the pores and deformation of the morphology in course of the calcination/thermal conversion, the reported flux-assisted solution-based thermal conversion route here was also believed helpful for the preparation of other pore-free 1D nanostructures with high crystallinity and well-preserved 1D morphology via dehydration or devolatilization of the corresponding 1D nanostructured precursors.

Acknowledgment. This work was supported by the National Natural Science Foundation of China (No. 50574051) and the Open Foundation of Tsinghua University. We thank Prof. Xun Wang at the Department of Chemistry, Tsinghua University, China, for his helpful discussion, and we also appreciate the editor and reviewers for their instructive suggestions on the great improvement of the work.

Supporting Information Available: XRD patterns of the washed and unwashed hydrothermal product (Figure S1), EDS spectrum recorded from the irregular block particles during the SEM observation (Figure S2), and the successively captured images recorded by the CCD camera showing the melting behavior of the block NaCl under the electron beam bombardment (Figure S3). This material is available free of charge via the Internet at http://pubs.acs.org.

References

(1) Li, Y. D.; Wang, J. W.; Deng, Z. X.; Wu, Y. Y.; Sun, X. M.; Yu, D. P.; Yang, P. D. *J. Am. Chem. Soc.* **2001**, *123*, 9904.
(2) Pan, Z. W.; Dai, Z. R.; Wang, Z. L. *Science* **2001**, *291*, 1947.
(3) Xia, Y. N.; Yang, P. D.; Sun, Y. G.; Wu, Y. Y.; Mayers, B.; Gates, B; Yin, Y. D.; Kim, F; Yan, H. Q. *Adv. Mater.* **2003**, *15*, 353.
(4) Caussat, B.; Vahlas, C. *Chem. Vap. Deposition* **2007**, *13*, 443.
(5) Wang, X. Ph.D. Thesis, Tsinghua University, China, 2004.
(6) Tas, A. C. *J. Am. Ceram. Soc.* **2001**, *84*, 295.
(7) Liu, Y. K.; Wang, G. H.; Xu, C. K.; Wang, W. Z. *Chem. Commun.* **2002**, *14*, 1486.
(8) Li, Y.; Wang, J.; Deng, Z.; Wu, Y.; Sun, X.; Yu, D.; Yang, P. *J. Am. Chem. Soc.* **2001**, *123*, 9904.
(9) Mo, M.; Zeng, J.; Liu, X.; Yu, W.; Zhang, S.; Qian, Y. *Adv. Mater.* **2002**, *14*, 1658.
(10) Li, Y. D.; Li, X. L.; He, R. R.; Zhu, J.; Deng, Z. X. *J. Am. Chem. Soc.* **2002**, *124*, 1411.
(11) Wang, X.; Zhuang, J.; Chen, J.; Zhou, K.; Li, Y. *Angew. Chem., Int. Ed.* **2004**, *43*, 2017.
(12) Yoshimura, M.; Byrappa, K. *J. Mater. Sci.* **2008**, *43*, 2085.
(13) Du, N.; Zhang, H.; Chen, B. D.; Wu, J. B.; Li, D. S.; Yang, D. R. *Nanotechnology* **2007**, *18*, 065605.
(14) Fang, Y. P.; Xu, A. W.; You, L. P.; Song, R. Q.; Yu, J. C.; Zhang, H. X.; Li, Q.; Liu, H. Q. *Adv. Funct. Mater.* **2003**, *13*, 955.

(15) Wang, X.; Sun, X. M.; Yu, D. P.; Zou, B. S.; Li, Y. D. *Adv. Mater.* **2003**, *15*, 1442.
(16) He, Y.; Tian, Y.; Zhu, Y. F. *Chem. Lett.* **2003**, *32*, 862.
(17) Xu, A. W.; Fang, Y. P.; You, L. P.; Liu, H. Q. *J. Am. Chem. Soc.* **2003**, *125*, 1494.
(18) Yang, Z. H.; Zhang, H. C.; Zhang, W. X.; Wang, X.; Qian, Y. T.; Wen, X. G.; Yang, S. H. *J. Solid State Chem.* **2006**, *179*, 679.
(19) Li, Y.; Zhuang, J.; Sun, X. M.; Deng, Z. X.; Li, Y. D. *Mater. Chem. Phys.* **2002**, *76*, 119.
(20) Shen, S. C.; Chen, Q; Chow, P. S.; Tan, G. H.; Zeng, X. T.; Wang, Z.; Tan, R. B. H. *J. Phys. Chem. C* **2007**, *111*, 700.
(21) Ma, M. G.; Zhu, Y. J.; Xu, Z. L. *Mater. Lett.* **2007**, *61*, 1812.
(22) Gao, X.; Zhu, H.; Pan, G.; Ye, S.; Lan, Y.; Wu, F.; Song, D. *J. Phys. Chem. B* **2004**, *108*, 2868.
(23) Huang, B.; Liu, Z.; Hong, J. M.; Chen, X. T.; Xue, Z. L.; You, X. Z. *J. Cryst.Growth* **2005**, *276*, 613.
(24) Zhang, Y. C.; Qiao, T.; Hu, X. Y.; Zhou, W. D. *J. Cryst. Growth* **2005**, *280*, 652.
(25) Xu, R.; Zeng, H. C. *J. Phys. Chem. B* **2003**, *107*, 12643.
(26) Li, L. R.; Wang, W. Z. *Solid State Commun.* **2003**, *127*, 639.
(27) Wang, W. Z.; Liu, Y. K.; Xu, C. K.; Zheng, C. L.; Wang, G. H. *Chem. Phys. Lett.* **2002**, *362*, 119.
(28) Xu, C. K.; Xu, G. D.; Liu, Y. K.; Zhao, X. L.; Wang, G. H. *Scr. Mater.* **2002**, *46*, 789.
(29) Ma, R. Z.; Bando, Y.; Sato, T. *Appl. Phys. Lett.* **2002**, *81*, 3467.
(30) Ma, R. Z.; Bando, Y.; Golberg, D.; Sato, T. *Angew. Chem., Int. Ed.* **2003**, *42*, 1836.
(31) Zhang, J.; Zhao, Y. M. *Acta Phys.-Chim. Sin.* **2006**, *22*, 110.
(32) Li, Y.; Fan, Z. Y.; Lu, J. G.; Chang, R. P. H. *Chem. Mater.* **2004**, *16*, 2512.
(33) Zeng, Y.; Yang, H.; Fu, W.; Qiao, L.; Chang, L.; Chen, J.; Zhu, H.; Li, M.; Zou, G. *Mater. Res. Bull.* **2008**, *43*, 2239.
(34) Elssfah, E. M.; Elsanousi, A.; Zhang, J.; Song, H. S.; Tang, C. C. *Mater. Lett.* **2007**, *61*, 4358.
(35) Sakane, K.; Kitamura, T.; Wada, H.; Suzue, M. *Adv. Powder Technol.* **1992**, *3*, 39.
(36) Kitamura, T.; Sakane, K.; Wada, H. *J. Mater. Sci. Lett.* **1988**, *7*, 467.
(37) Sakane, K.; Wada, H.; Kitamura, T.; Suzue, M. *Gypsum Lime* **1991**, *235*, 16.
(38) Liu, Y. S. *Acta Petrol. Mineral. Anal.* **1982**, *1*, 30.
(39) Liu, Z. H.; Hu, M. C. *Thermochim. Acta* **2004**, *411*, 27.
(40) Liang, J. H. Ph.D Thesis, Tsinghua University, China, 2005.
(41) Zhu, W. C.; Xiang, L.; He, T. B.; Zhu, S. L. *Chem. Lett.* **2006**, *35*, 1158.
(42) Xie, X. D.; Zheng, M. P.; Liu, L. B. *Borates Minerals*; Science Press: Beijing, 1965; pp 54−57.
(43) Liu, Z. H.; Hu, M. C.; Gao, S. Y. *J. Therm. Anal. Calorim.* **2004**, *75*, 73.
(44) Guo, C. G.; Cheng, W. D.; Chen, J. T.; Huang, J. S.; Zhang, Q. E. *Acta Crystallogr.* **1995**, *C51*, 351.
(45) Suryanarayana, C.; Grant Norton, M. *X-Ray Diffraction, a Practical Approach*; Plenum Press: New York, 1998.
(46) Sun, Y. G.; Yin, Y. D.; Mayers, B. T.; Herricks, T.; Xia, Y. N. *Chem. Mater.* **2002**, *14*, 4736.
(47) Jiang, X. C.; Herricks, T.; Xia, Y. N. *Nano Lett.* **2002**, *2*, 1333.

CG800050U